Synthesis, Characterization, and Biological Activity of $WO_3/TiO_2/CeO_2$ Ternary Nanocomposites

T. Kousalya[1], D. Vijayalakshmi[1,*], N. Karthikeyan[2], Riya[3]
[1,3]Department of Physics, VELS Institute of Science, Technology & Advanced Studies (VISTAS), Pallavaram, Chennai, Tamil Nadu 600117
[2]Department of Physics, College of Engineering, Anna University, Chennai 600025, India
[*]**Corresponding Author:** D. Vijayalakshmi.
Email: vijayalakshmi.sbs@vistas.ac.in, viji.duraikannu@gmail.com

ABSTRACT
A $WO_3/TiO_2/CeO_2$ ternary metal oxide nanocomposite was synthesized through a co-precipitation and hydrothermal approach and comprehensively characterized to evaluate its structural, optical, morphological and antimicrobial properties. X-ray diffraction (XRD) analysis revealed the formation of monoclinic WO_3, rutile TiO_2 and cubic fluorite CeO_2 phases, consistent with standard JCPDS data, indicating high phase purity of the synthesized materials. Fourier transform infrared spectra (FTIR) revealed characteristic metal-oxygen vibrational modes, indicating effective coupling and integration of the constituent oxides. Ultra violet (UV)-Visible spectroscopy was used to analyze the optical response of the nanocomposites and high-resolution scanning electron microscopy (HRSEM) coupled with energy-dispersive X-ray (EDX) analysis was carried over to evaluate surface morphology and elemental composition. The antibacterial activity of the synthesized nanocomposites was assessed against Streptococcus mutans and Salmonella typhi, while antifungal activity was examined against Candida albicans and Aspergillus niger. Overall, the results highlight the broad-spectrum antimicrobial potential of the $WO_3/TiO_2/CeO_2$ nanocomposites for prospective biomedical and environmental applications.
Keywords: $WO_3/TiO_2/CeO_2$ nanocomposites, ternary metal oxide, Antibacterial activity, Gram-positive bacteria, Gram-negative bacteria, Antifungal activity.
How to cite this article: Kousalya T, Vijayalakshmi D, Karthikeyan N, Riya. Synthesis, Characterization, and Biological Activity of $WO_3/TiO_2/CeO_2$ Ternary Nanocomposites. Int J Drug Deliv Technol. 2026;16(48s): 426-441. DOI: 10.25258/ijddt.16.48s.43
Source of support: Nil.
Conflict of interest: None

1. INTRODUCTION

Microbial contamination in daily surroundings and industrial facilities remains a persistent threat to human health and product quality, highlighting the growing need for effective strategies to control harmful microorgansims. Numerous pathogenic bacteria including *Escherichia coli, Klebsiella pneumoniae, Pseudomonas aeroginosa, Streptococcus mutans, Staphylococcus aureus, and Salmonella typhi* are frequently detected in water, soil and air, can cause the foodborne disease, respiratory complications and urinary tract infection [1-2]. In addition to bacterial pathogens, fungal species such as *Candida albicans* *and Aspergillus niger* are routinely monitored due to their role in opportunistic and systems infections. The widespread presence of these microorganism underscores their impact on public health and highlights the neccessity for advanced antimicrobial material capable of limiting their proliferation [3].

Metal oxides including ZnO, CuO, TiO_2, AgO, La_2O_3, Fe_2O_3, Co_3O_4, CeO_2, WO_3, SnO_2, Nb_2O_5, and SrO are widely recognized for the strong metal-oxygen interactions, structural stability and inherent antimicrobial properties, making them attractive candidates for microbial control application [4,5]. Among various synthesis routes, the co-percipitation methods is particularly advantageous for producing uniform metal oxides materials, as it enables the simultaneous precipitation of metal ions using an appropriate precipitation agents, followed by filtration, drying, and calcination to yield the final nanaostructured products [6].

WO_3 contributes chemical stability, enhanced surface activity, and robust structural properties, making it an effective component in antimicrobial metal oxide systems. TiO_2 is well known for its excellent biocompatibility and broad-spectrum antibacterial activity, which further strengthens the antimicrobial performances of mixed oxide materials. CeO_2 with its remarkable redox behavior, high oxygen storage capable, structural reliability, adds additional functionality to these oxides and enhances their suitable for multifunctional antimicrobial systems [7-10]. When integrated into a composites, TiO_2, WO_3, and CeO_2 can work synergistically, improving surface characteristics charge distrubution, and overall functional performance compared to their individual counterparts [11-12].

In this present work a $WO_3/TiO_2/CeO_2$ nanocomposites was synthesized via the co-percipitation technique and evaluated for its antimicrobial activity against selected microorganisms. This antibacterial activity assessed to focused on Gram-positive *S. mutans* , Gram-negative *S. typhi,* and the fungal strains *Candida albicans* and *A.niger,* enabling the determination of the composite's potential broad-spectrum antibacterial and antifungal activities. Detailed structural, optical, elemental, and physicochemical analyses were performed to characterize the synthesized material and to understand the factors governing its antimicrobial behavior.

2. Experimental Section

2.1 Methods and materials

Ammonium tungstate hydrate, sodium tungstate dihydrate, nitric acid, Cerium (III) nitrate hexahydrate ($Ce(NO_3)_3.6H_2O$;99.99%), titanium tetraisopoxide (TTIP), 2- propanol, hydrochloric acid, were procured from Sigma-Aldirch, while sodium hydroxide (NaOH;99%) and hydrochloric acid (HCl) were brought from merck. All other chemicals used in the experiments were of analytical grade and were utilized as received without additional impurities.

2.2 Preparation of WO_3 Nanoparticles

WO_3 nanoparticles were synthesized using co-percipitation technique. Briefly, 0.032 g of ammonium tungstate hydrate was dissolved in 67 mL of deionized water and stirred for 2 h to ensure complete dissolution. Precipitation was induced by the gradual dropwise addition of 50 mL of HNO_3 under continous stirring. The suspension was then heated at 80 °C for 40- 70 min with constant agitation (800 rpm) and subsequently kept undisturbed for 24 h to allow particles growth and sedimentation. The resulting precipiatate was separated by decantation, thoroughly washed with deionized water to remove unwanted ions, and dried at 80 °C in a hot oven. The dried sample was finally calcined at 800 in muffle furnace to obtain well- crystallized WO_3 nanoparticles.

2.3 Preparation of TiO_2 Nanoparticles

TiO_2 nanoparticles were prepared by hydrothermal route. In this process, 4.9 mL of titanium tetraisopropoxide (TTIP) was added into 50 mL of distilled water and stirred for 2 h to form a homogenous precursor solution. Subsequently, 20 g of NaOH was added dropwise in the precipiate solution. The obtained mixture was tranferred into Telfon-lined stainless-steel autoclave, and heated at 200°C for 48 h. After naturally cooling to room temperature, the solid product was filtered and acid-washed with 25 mL of HCl (pH 2) for 30 min followed by repeated washing with distilled water until neutral pH was reached. The precipitate solution was dried at 100 °C for 6 h, yielding TiO_2 nanoparticles suitable for further characterization and application.

2.4 Preparation of $WO_3/TiO_2/CeO_2$ Nanocomposites

A homogeneous suspension was prepared by dispersed 1 g of WO_3, 1g of TiO_2, and 1g of CeO_2 in distilled water under continuous stirring to ensure unifrom mixing of the oxide powders. Sodium hydroxide solution was then added dropwise until the pH reached 7-10 facilitating complete precipitation of the metal oxides species. The resulting mixture was then transferred into Telfon-lined stainless steel autoclave heated at 120°C for 6-12 h to promote crystallization and the initial formation of the ternary composites structure. And settled at the room temperature, the obtained product was thoroughly washed with distilled water to remove residual ions and impurities, and then dried in a oven at 60-80 °C to eliminate moisture. Finally, the dried sample was annealed at 400°C for 4h, enhancing crystallinity and interfacial bonding, thereby yielding the $WO_3/TiO_2/CeO_2$ nanocomposites [14].

2.5 Characterization Techniques

The physical and morphological properties of the synthesized materials were synthesized using various advanced characterisation techniques. Powder X-ray diffraction (XRD) pattern were recorded using a Burker D8 Advance diffractometer equipped with Cu kα radiation (λ=1.5406Å) to analyse the crystalline phases and structural characteristics. Fourier Transform Infrared (FTIR) spectra were obtained using a Perkin Elmer Spectrum 2 spectrometer to identify functional group and chemical bonding features. The absorption and transmission of optical bandgap was assessed using an Ocean Optics UV-Vis spectrospectrocopy. The surface morphology and particles distribution were investigated using high-resolution scanning electron microscopy (HRSEM) coupled ewith energy-dispersive spectroscopy (EDX) on FEI Quanta 200 instrument operated at 25kV, enabling detalied evaluating of the size of the nanostructure and elemental composition of the synthesised samples **[13].**

2.6 Antimicrobial activity

The antibacterial activity of the synthesized samples was assessed using the agar well-diffusion method, with streptomycin (1mg/ml - 20 µl) employed as the positive control. Antibacterial performance was evaluated against the Gram-positive *S. mutans* and the Gram-negative *S. typhi* at concentrations of 125 µg/mL, 250 µg/mL, 500 µg/mL, 1000 µg/mL. Antifungal activity against *C. albicans* and *A. niger* was examined at the same concentrations using the well-diffusion methods on potato dextrose agar (PDA) medium, with *ketoconazole* (1mg/ml - 20 µl). Nutrient agar plates were inoculated with the respective microbial strains and unifromly spread to ensure consistent growth. Wells of 6mm diameter were then made using a sterile cork borer, and the prepared sample were the zones of inhibition were measured and recorded following the protocol described by [15]**.**

3. Result and Discussion

3.1 XRD analysis

Powder X-ray diffraction (XRD) analysis was performed using a bruker AXS D8 Advance diffractometer equipped with Cu Kα radiation (λ = 1.5406), and the diffraction patterns were recorded over a 2θ range of 10-80°. **Figure (1a-1d)** present the XRD patterns of pure WO_3, TiO_2, CeO_2, and the ternary $WO_3/TiO_2/CeO_2$ nanocomposites. As illustrated in **(Figure 1a)**, WO_3 exhibit distinct reflections indexed to the monoclinic phase, corresponding to the (002), (020), (012), (211), (202), (112), (222), (014), (232), (402), (341) planes, consistent with JCPDS No. 83-0950. The XRD pattern of TiO_2 **(Figure 1b) (Figure 1b)** display sharp and intense peaks assigned to the (110), (200), (210), (211), (002), (311), and (112) planes, confirming the formation of the rutile polymorph (JCPDS No. 75-1537) [16]. The diffraction pattern of CeO_2 nanoparticles **(Figure 1c)** reveals characteristic reflections corresponding to the (111), (200), (220), (311), (222), (400), (331), and (420) planes indicating the formation of the cubic fluorite structure and aligning well with reportes [17,18]. The crystallite size of WO3, TiO2 and CeO_2 was calculated using the Debye-Scherrer equation:

$$D = \frac{0.98\,\lambda}{B\ \ Cos\ \theta}$$

In the Scherrer equation, λ represents the X-ray wavelength, β is the full width at half maximum (FWHM), and θ is the Bragg angle. The calculated the average crystallite size for WO_3, TiO_2, and CeO_2 nanoparticles was estimated to be approximately 87 nm, 42 nm 25 nm, respectively [19].

The XRD profile of the ternary $WO_3/TiO_2/CeO_2$ nanocomposites **(Figure 1d)** displays a combination of diffraction peaks from monoclinic WO_3, rutile TiO_2, and cubic CeO_2, without any defectable secondary phases [20]. The average crystallite size of the approximately 32 nm, indicating the formation of well-defined nanocrystalline domains. The presence of sharp and intense diffraction peaks further demonstrates that the individual crystalline structures of WO_3,TiO_2, CeO_2 retained during composite formation, reflecting the high structural integrity and phase stability of the ternary system [21].

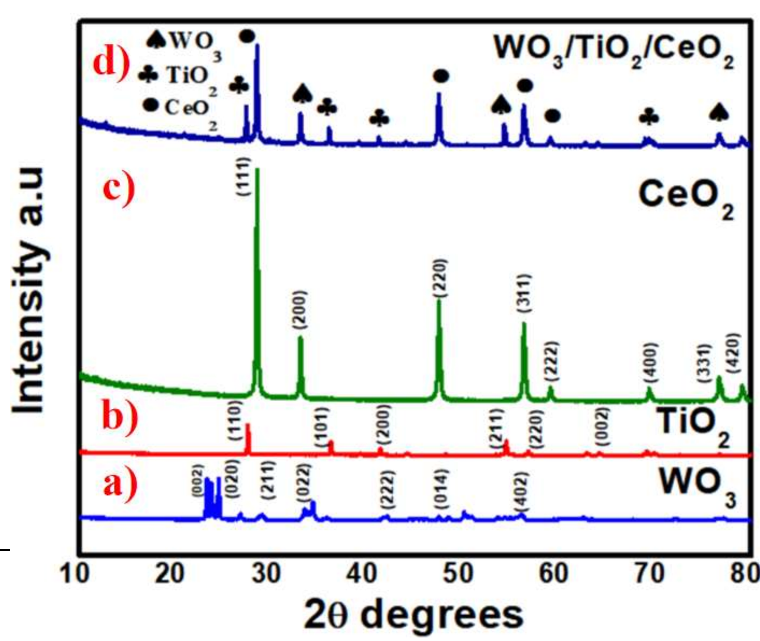

Figure 1a-1d: X-ray diffraction patterns of pristine WO_3, TiO_2, CeO_2, and the $WO_3/TiO_2/CeO_2$ nanocomposite.

3.2 FTIR Analysis

FTIR spectroscopy of WO_3,TiO_2,CeO_2 and $WO_3/TiO_2/CeO_2$ nanocomposites in the range of 400-4000 cm^{-1} reveals the characteristic vibrational features of each oxide, indicating proper formation of the materials as shown in **Figure 2a-2d** [21]. In the case of **Figure 2a** WO_3 a band at 3370 cm^{-1} corresponds to O-H stretching, confirming surface hydroxyl groups [22], while band at 1615 cm^{-1} and 1406 $cm^{-1}$are assigned to H-O-H bending of adsorbed water and W-O-H vibrations, respectively [23]. TiO_2 shows a similar O-H stretching at 3374 cm^{-1}, bending at 1640cm^{-1} and Ti-O bending at 480 cm^{-1}, confirming structural integrity are represented in **Figure 2b** [24-25]. The FTIR spectrum of CeO_2 exhibit a Ce-O stretching peaks at 716 cm^{-1}, broad O-H stretching at 3342cm^{-1} [26,27], and surface hydroxyl at 3725cm^{-1} [28], confirmining its metal oxide structure and surface functionality as shown in **Figure 2c**. For the $WO_3/TiO_2/CeO_2$ nanocomposites,in **Figure 2d** peaks at 498 cm^{-1}, 687 cm^{-1} and 869 cm^{-1} correspond to Ce-O, Ti-O-Ti/W-O-Ti and W-O-W vibration, respectivley [29,30] while O-H bending at 1673 cm^{-1} and broad O-H stretches at 3358 cm^{-1} and 3771 cm^{-1} confirm the presence of surface hydroxly group [31]. These observation indicate that the ternary nanocomposites retain surface hydroxyl functionalities and exhibit strong interaction among the metal oxides, which are advantageous for antimicrobial activity anf surface-related application [32].

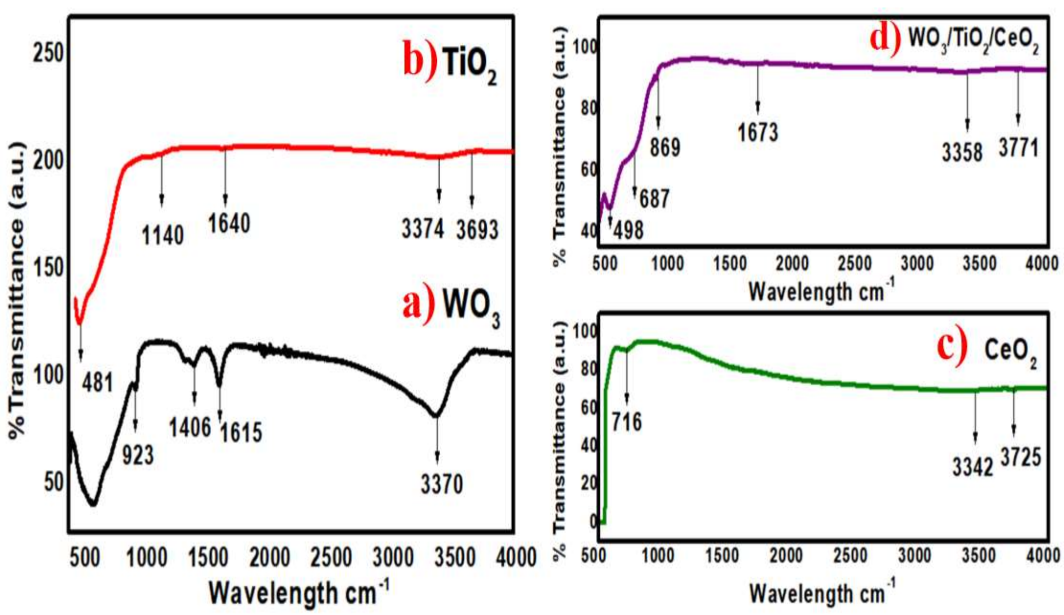

Figure 2a-2d: FTIR spectra of (a) WO_3, (b) TiO_2, (c) CeO_2, and (d) $WO_3/TiO_2/CeO_2$ nanocomposite, showing the characteristic vibrational modes of each oxide

3.3 UV-Visible spectroscopy

The optical obsorption characteristics of WO_3, TiO_2, CeO_2 and the $WO_3/TiO_2/CeO_2$ nanocomposites were systematically analyzed by UV-Vis absorption spectroscopy in the range of 200-800 nm. As shown in **Figure 3a-3d,** the WO_3 exhibits a well defined absortion edge at approximately 380 nm, indicating its predominant response in the ultraviolet region, whereas TiO_2 shows an absorption onset near 400 nm, characteristics of its wide band gap semiconductor behavior. In this case CeO_2 nanoparticles also display a strong absorption edge around 380 nm, accompanied by slight spectral shift that can be attributed to size effects and defect -induced electronic states. In contrast, the $WO_3/TiO_2/CeO_2$ ternary nanocomposites demonstates a noticeable extension of absorption into the visible region, suggesting enhanced light- harvesting capability arising from effective interfactial coupling and heterojunction formation among the consitutent oxides.

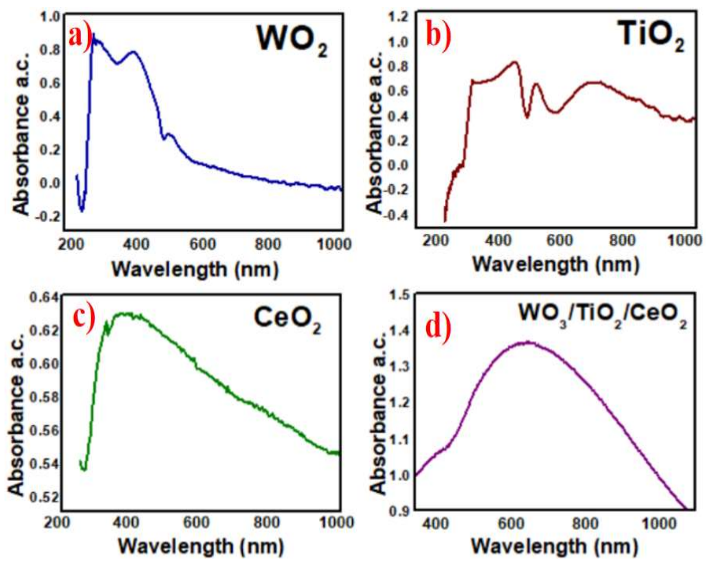

Figure 3a-3d: UV-Vis absorption spectra of (a) WO_2, (b) TiO_2, (c) CeO_2, and (d) $WO_3/TiO_2/CeO_2$ nanocomposite.

The optical band gap energies were evaluated using the Tauc plotting $(\alpha h\upsilon)^2$ as a function of photon energy ($h\upsilon$), assuming direct allowed electronic transitions as presented in **Figure 4e-4h**. From the linear extrapolation of these plots, band gap values of 2.26 eV for WO_3, 2.44 eV for TiO_2 and significantly reduced value of 1.07 eV for CeO_2 were obtained confirming the role of oxygen vacanies and annealing- induced defects states in band gap narrowing [33-34]. The $WO_3/TiO_2/CeO_2$ nanocomposites exhibits an optical band gap of 2.60 eV, as shown in **Figure 4h** reflecting a modified structure and favorable band alignment resulting from the combined presence of multiple oxides phases [35].

ZZ

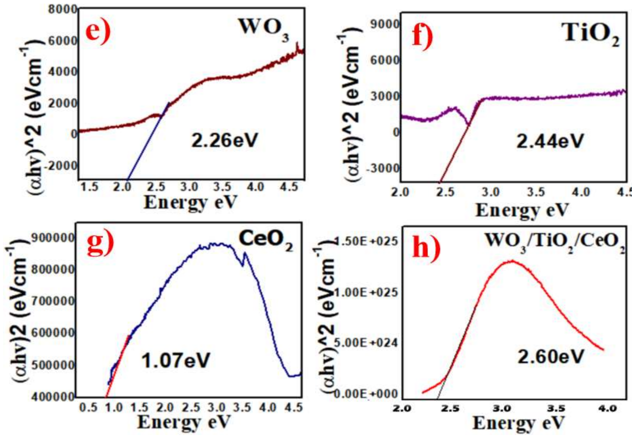

Figure 4e–4h. Tauc plots of (e) WO_3, (f) TiO_2, (g) CeO_2, and (h) $WO_3/TiO_2/CeO_2$ nanocomposite, showing the determination of their optical band gap

3.4 HRSEM

High-Resolution Scanning Electron Microscopy (HR-SEM; FEI Quanta 200f), was employed to examine the surface morphology of the synthesized nanostructures, and the corresponding micrographs are presemted in **Figure 5(a-d)**. These images clearly highlight the distinct morpholofical features of the individual oxides and the ternary $WO_3/TiO_2/CeO_2$ nanocomposite, which collectively influence their antimicrobial performance. As observed in **Figure 5a**, monoclinic WO_3 exhibit irregular granular particles with rough surface and moderate agglomeration, with an average particles size of approximately 37 nm suggesting a relativley high surface area that factilitates enhanced microbial interaction. In **Figure 5b**, rutile phase TiO_2 shows nearly spherical, uniformly dispersed nanoparticles with smooth surface, and as average particles size od approximately 34 nm, indicating [36]. of a high surface-to-volume ratio favourable for enhanced biological activity. The SEM micrograph of CeO_2 in **Figure 5c** reveals predominantly spherical shape with improved homogensiry and reduced agglomeration, possessing an average particles size of approximately 22 nm, which reflects the formation of well- defined nanoparticles cluster that enhances surface reactivity.

In the $WO_3/TiO_2/CeO_2$ **(Figure 5d),** the morpholoy appeard as densely interconnected network of mixed oxide nanoparticles, where the granular WO_3 particles and spherical TiO_2 and CeO_2 domains are uniformly distributed. The average particles size of $WO_3/TiO_2/CeO_2$ nanocomposites is approximately 27 nm, comfirming their nanoscale nature. This well- integrated architecture increase surface roughness, provide additional active sites, and enhances the overall contact interface with microbial cell contributing to improved antimicrobial efficacy

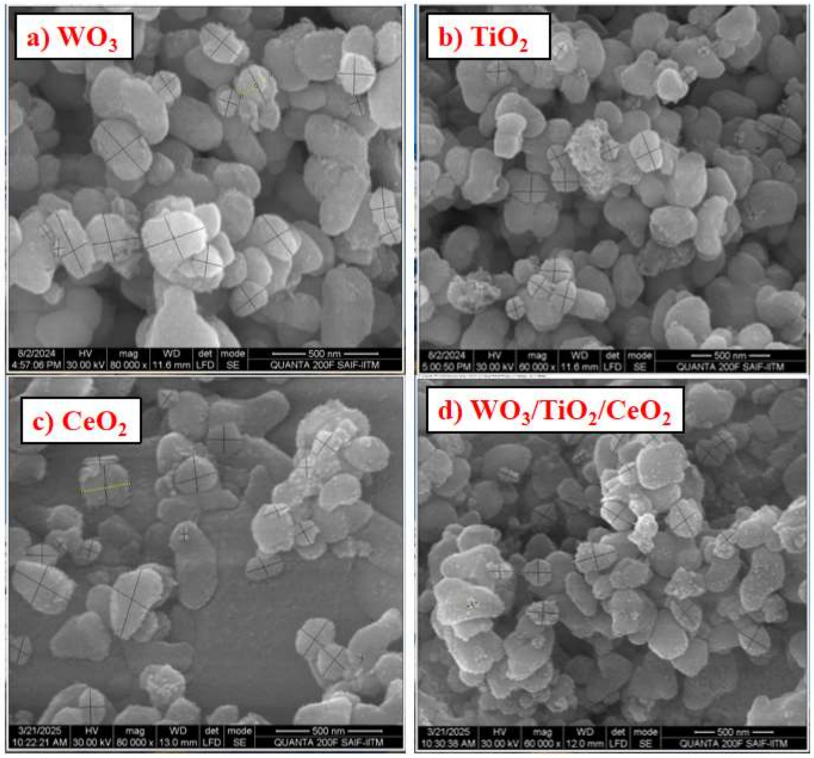

Figure 5a–5d: HRSEM images of (a) WO_3, (b) TiO_2, (c) CeO_2, and (d) $WO_3/TiO_2/CeO_2$ nanocomposite, showing the morphology and particle distribution of individual oxides and the ternary heterostructure.

3.5 EDX ANALYSIS

The elemental composition of the synthesized WO_3,TiO_2,CeO_2, and $WO_3/TiO_2/CeO_2$ nanocomposite samples was analyzed using energy-dispersive X-ray specrtroscopy (EDX), and the corresponding spectra are presented in **Figure 6a-6d.**

The EDX spectrum of WO_3 revealed well-defined peaks corresponding exclusively to tungsten (W) and oxygen (O), comfirming the high purity and successful formation of tungsten oxide [37]. Similarly, the TiO_2 sample exhibited characteristics Ti and O signal, consistent with expected stoichiometry of titianium dioxide [38]. In the case of CeO_2 distinct and clear peaks associated with cerium and oxygen were observed, confirming the succesful formation of cerium oxide without any additional undersired signals. The ternary $WO_3/TiO_2/CeO_2$ nanocomposites displayed combined elemental peaks of W, Ti, Ce, and O, the successful incorporation of all three metal oxides into the heterostructure, while the corresponding weight and atomic percentages further validate their the proper composition and homogeneous distribution. Overall, the EDX result confirm the elemental purity of the individual oxides and substaniate the effective formation of the $WO_3/TiO_2/CeO_2$ ternary composite.

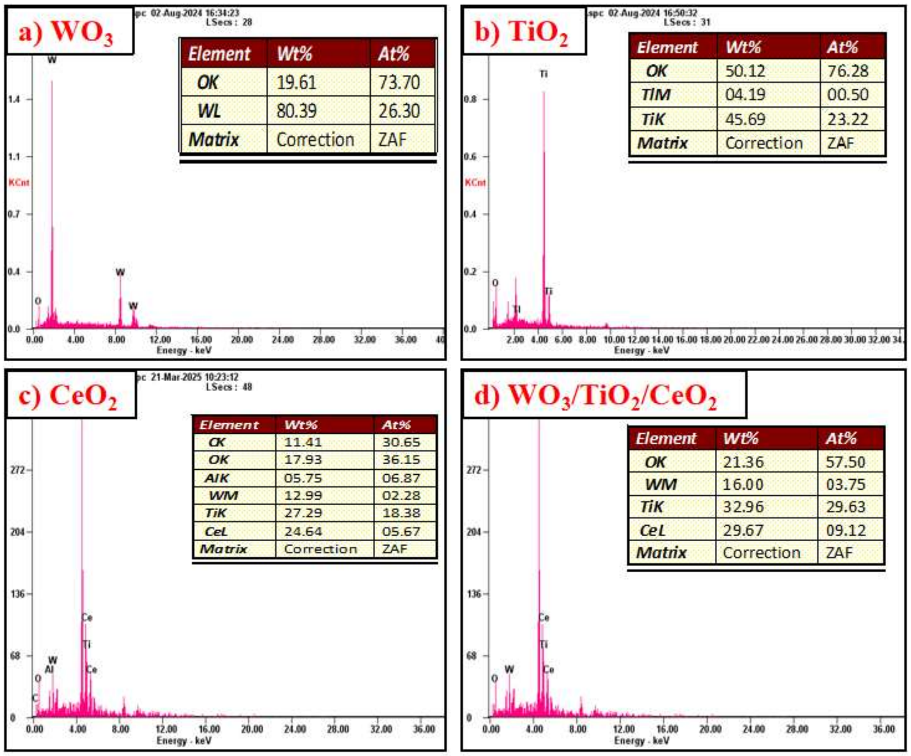

Figure 6a–6d. EDX spectra of (a) WO_3, (b) TiO_2, (c) CeO_2, and (d) $WO_3/TiO_2/CeO_2$ nanocomposite.

4. Antimicrobial activity

4.1 Antibacterial activity

The antibacterial activity of the syntheisized $WO_3/TiO_2/CeO_2$ nanocomposites was evaluated in vitro using the agar well diffusion method against Gram-positive *Streptococcus mutans* and Gram-negative *Salmonella typhi.* The assay was performed at differnet concentration of the nanocomposite, namely 125 µg/mL, 250 µg/mL, 500 µg/mL, 1000 µg/mL,With DMSO as the negative control and Streptomycin as the positive control. The antibacterial efficacy was assessed by measuring the zone of inhibition (ZOI mm) after 24 h of incubation. The representation agar plates **(Figure 7a-7b)** clearly show well-defined inhibition zones surrounding the nanocomposites- loaded wells, confirming its antibacterial efficacy. As summarized in the quantitative inhibition date **(Table 1)** and the further illutrated in the comparative bar chart **(Figure 8)**, the nanocomposites exhibits a pronunced concentration- dependent antibacterial response. For *Salmonella typhi*, the zone of inhibition increases progressively from 9 mm at 250 µg/mL to 12 mm at 500 µg/mL and 15 mm at 1000 µg/mL, reaching a maximum inhibition zone of 28 mm at the higest effectibe concentration, with 13 mm and 21 mm zones, respectively. No inhibition was observed in the negative control, confirming that the antibacterial effect originates from the nanocomposites itself. The enhanced activity at higher concentration is attributed to the synergistic action of WO_3, TiO_2 and CeO_2, which promotes strong interaction with bacterial cell membrances, leading to membranes, leading to membrane disruption and oxidative stress-induced cellular damage. Notably, the nanocomposite demonstrates greater antibacterial effectiveness against Gram-negative *Salmonella typhi* than Gram-positive *Streptococcus mutans*, which is consistent with differences in cell wall structure **[35,36]**. Overall, the combined evidence from the antibacterial images, inhibition table, and bar chart confirms that the $WO_3/TiO_2/CeO_2$ nanocomposites possesses strong and concentration-dependent antibacterial activity, highlighting its potenial for antimicrobial and biomedical applications [37].

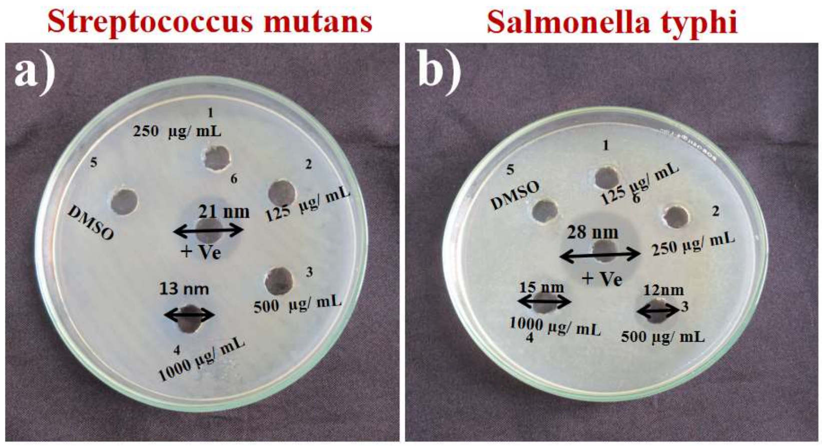

Figure 7a-7b: Antibacterial activity of the $WO_3/TiO_2/CeO_2$ nanocomposite against *Streptococcus mutans* and *Salmonella typhi* at different concentrations.

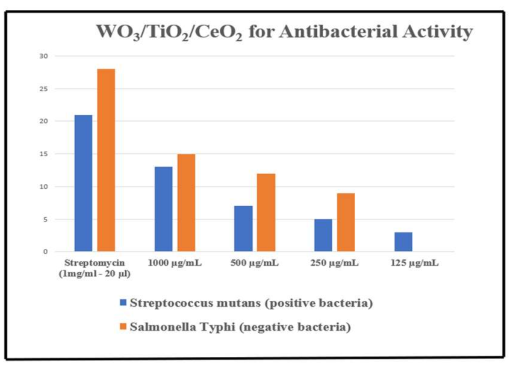

Figure 8. Agar well diffusion assay showing antibacterial activity of the $WO_3/TiO_2/CeO_2$ nanocomposite against (a) *Streptococcus mutans* and (b) *Salmonella typhi*.

Table 1. Zone of inhibition (mm) of the $WO_3/TiO_2/CeO_2$ nanocomposite against *Streptococcus mutans* and *Salmonella typhi*.

oorganisms	**Zone of Inhibition in mm**					

onella typhi						
tococcus mutants						

4.2 Antifungal activity

The antifungal efficacy of the $WO_3/TiO_2/CeO_2$ nanocomposites was systematically evaluated in vitro using the agar well diffusion method against the pathogenic fungal strains *Candida albicans* and *Aspergillus niger* at concertrations of 125 µg/mL, 250 µg/mL, 500 µg/mL and 1000 µg/mL with DMSO used as the negative control and streptomycin as the postrive control. The representative antifungal agar plates **(Figure 9a-9b)** clearly show well-defined zones of inhibition around the nanocomposite-loaded wells, confirming its effective antifungal activity against both fungal strains, while the absence of inhibition in the DMSO control confirms that the observed antifungal effect originates solely from the nanocomposite. Quantitative inhibition data summarized in **Table 2** and further illustrated in the comparative bar chart **(Figure 10)** reveal a clear concentration-dependent antifungal response, with *candida albicans* showing moderate inhibition at lower concentrations and a maximum zone of inhibition of 31 mm at 1000 µg/mL, indicating strong antifungal susceptibility, whereas *Aspergillus niger* exhibits comparatively lower sensitivity, achieving a maximum inhibition zone of 11mm at the highest concentration, which can be attributed to its filamentous structure and stronger cell well defenses. The bar chart clearly highlights the superior antifungal performance of the nanocomposite against *Candida albicans* compared to *Aspergillus niger*, demonstrating strain-dependent activity. The enhanced antifungal efficacy at higher concentrations is attributed to the synergistic interaction of WO_3, TiO_2 , CeO_2, which promotes increased generation of reactive oxygen species (ROS), disruption of fungal cell membranes, leakage of intracellular constituents, and oxidative stress-induced damage to essential biomolecules, consistent with perviously reported metal oxide- based antifungal mechanisms [38-43]. Overall, the combined that the $WO_3/TiO_2/CeO_2$ nanocomposites exhibits significant and concentration-dependent antifungal activity, highlighting its strong potential for antifungal, biomedical, and antimicrobial surface- coating applications.

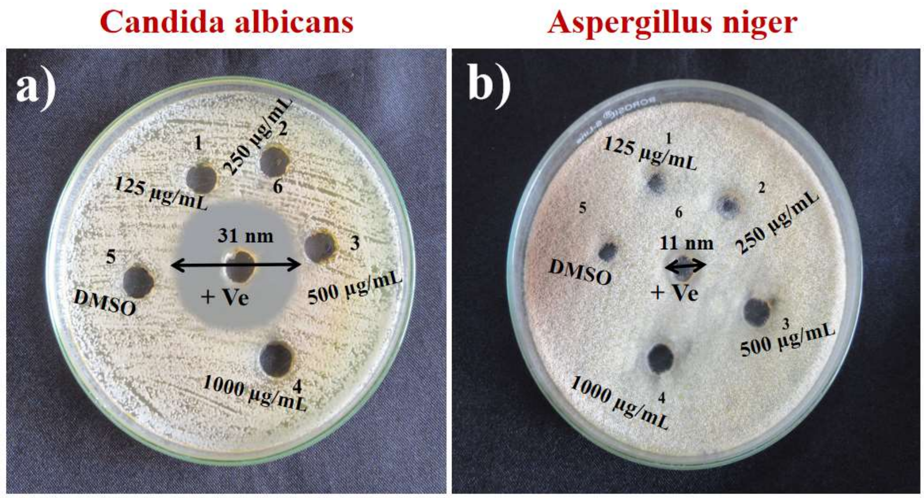

Figure 9a-9b. Comparative antifungal activity of the $WO_3/TiO_2/CeO_2$ nanocomposite against *Candida albicans* and *Aspergillus niger* at different concentrations.

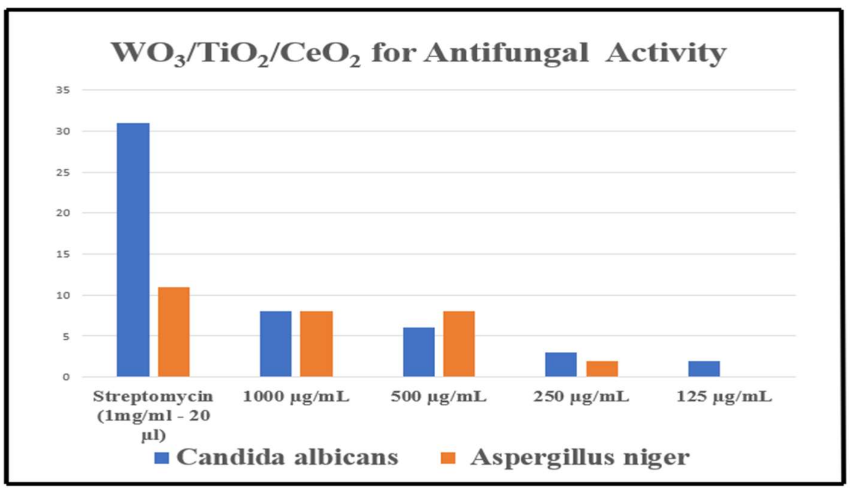

Figure 10. Agar well diffusion assay showing the antifungal activity of the $WO_3/TiO_2/CeO_2$ nanocomposite against (a) *Candida albicans* and (b) *Aspergillus niger*.
Table 2. Zone of inhibition (mm) of the $WO_3/TiO_2/CeO_2$ nanocomposite against *Candida*
albicans and *Aspergillus niger*.

roorganisms	**Zone of Inhibition in mm**					
dida albicans						

rgillus niger						

5. Conclusion

In conclusion WO_3, TiO_2, and CeO_2 nanoparticles and their ternary $WO_3/TiO_2/CeO_2$ nanocomposite were successfully synthesized via the co-percipitation and hydrothermal methods. X-ray diffraction (XRD) analysis revealed the formation of monoclinic WO_3, rutile-phase TiO_2, and cubic fluorite-structure for CeO_2, with the average crystallite sizes of approximately 87 nm, 42 nm, and 25 nm, respectively. Fourier transform infra-red (FTIR) analysis revealed characteristic metal-oxygen vibrational bands corresponding to Ce-O, Ti-O-Ti/W-O-Ti and W-O-W bonds, indicating effective coupling and strong interfacial, interaction among the constituent oxides. Ultra Violet (UV) -Visible spectroscopy showed strong light absorption with a distinct edge near 380 nm corresponding to a direct band gap of approximately 3.26 eV for $WO_3/TiO_2/CeO_2$ composites. High resolution-scanning electron microscope (HR-SEM) analysis comfirming the spherical shaped nanoparticles with high elemental purity, with an average particles sizes of 37 nm for WO_3, 34 nm for TiO_2, 22 nm for CeO_2 and 27 nm of the $WO_3/TiO_2/CeO_2$ nanocomposites approximately confirming nanoscale morphology and unifrom dispersion. Energy Dispersive X-Ray (EDX) further verified the presence of W, Ti, Ce and O without detectable impurities, indicating the successful formation and compositional purity of the ternary nanocomposite. Antimicrobial evalution demonstrated that the $WO_3/TiO_2/CeO_2$ nanocomposites exhibit significant antibacterial activity against Gram-positive (*Streptococcus mutans*) and Gram- negative (*Salmonella typhi*) strains, as well as notable antifungal activity against *Candida albicans* and *Aspergillus niger*, with C. albicans showing higer sensitivity, reflecting a species- dependent antimicrobial response. Overall, the ternary nanocomposites combine favorable structural, optical, and biological properties, highlighting their potential as effective antimicrobial agents for biomedical and envirinmental applications.

References

1) Marsh, P. D., & Zaura, E. Dental biofilm: ecological interactions in health and disease. Journal of Clinical Periodontology, (2017); 44(S18), S12–S22. https://doi.org/10.1111/jcpe.12679

2) Crump, J. A., & Mintz, E. D. Global trends in typhoid and paratyphoid Fever. Clinical Infectious Diseases, (2010);50(2), 241–246. https://doi.org/10.1086/649541

3) Brown, G. D., Denning, D. W., & Levitz, S. M. Tackling human fungal infections. Science, (2012); 336(6082), 647. https://doi.org/10.1126/science.1222236

4) World Health Organization. Global antimicrobial resistance and use surveillance. WHO Report. (2020); https://doi.org/10.46945/abcd.1234

5) Raghupathi, K. R., Koodali, R. T., & Manna, A. C. Size-dependent bacterial growth inhibition and mechanism of antibacterial activity of zinc oxide nanoparticles. Langmuir, (2011); 27(7), 4020–4028. https://doi.org/10.1021/la104825u

6) Palza, H. Antimicrobial polymers with metal nanoparticles. International Journal of Molecular Sciences, 2015;16(1), 2099–2116. https://doi.org/10.3390/ijms16012099

7) Gupta, S. M., & Tripathi, M. A review of TiO_2 nanoparticles. Chinese Science Bulletin, (2011); 56(16), 1639–1657. https://doi.org/10.1007/s11434-011-4476-1

8) Zhang, H., & Chen, G. Potent antibacterial activities of Ag/TiO_2

nanocomposite powders synthesized by a one-pot sol–gel method. Environmental Science & Technology,(2009); 43(8), 2905–2910. https://doi.org/10.1021/es803450f

9) Sheppard, L. R., et al. Functional properties of tungsten trioxide. Journal of Materials Chemistry A, (2015); 3(3), 1283–1290. https://doi.org/10.1039/C4TA04949A

10) Trovarelli, A. Catalytic properties of ceria and CeO_2-containing materials. Catalysis Reviews,(1996); 38(4), 439–520. https://doi.org/10.1080/01614949608006464

11) Mogensen, M., Sammes, N. M., & Tompsett, G. A. Physical, chemical and electrochemical properties of pure and doped ceria. Solid State Ionics, (2000); 129(1–4), 63–94. https://doi.org/10.1016/S0167-2738(99)00318-5

12) Yao, X., et al. Redox activity of cerium oxide nanoparticles: antibacterial and catalytic perspectives.Nanoscale (2013); 5(24), 11962–11969. https://doi.org/10.1039/c3nr04548k

13) Li, X., et al. Enhanced antibacterial performance of TiO_2-based composites. Journal of Alloys and Compounds, (2016);663, 165–172.

14) Yang, Y., Bian, X., Cai, M., & Wu, W. The Selective Catalytic Reduction Reaction and Mechanism of Citric Acid Modified the Ceo2-Wo3/Tio2 Catalyst. (2023); https://doi.org/10.2139/ssrn.4611832

15) Han, X., et al. Synergistic effects in mixed metal oxide nanocomposites for antimicrobial applications. Materials Science and Engineering: C, (2017);70, 303–310. https://doi.org/10.1016/j.msec.2016.08.081.

16) Sato, T., & Katayama, M. Indoor-Light-Activated Blue TiO_2-Molecule-WO_3 Visible-Light Photocatalyst Complex for Efficient Sterilization. ACS Omega, (2023); 8(17), 15023–15031. .https://doi.org/10.1021/acsomega.3c00856.

17) Baskar, G., Chandhuru, J., Fahad, K. S., Praveen, A. S., Chamundeeswari, M., & Muthu, T. S. Antimicrobial activity of metal oxide nanoparticles synthesized using biological methods. Journal of Chemical and Pharmaceutical Sciences, 1 (2017); 0(1), 447–451.

18) Azizi, R., Sayadi, M. H., & Shekari, H. Photocatalytic performance of WO_3/TiO_2 nanocomposites: synthesis, characterization, and application for dye degradation. Journal of Materials Science: Materials in Electronics,(2019); 30(12), 11345–11357.H.

19) M. Huang, S. Yu, B. Li, D. Lihui, F. Zhang, M. Fan, L. Wang, J. Yu, C. Deng,Influence of preparation methods on the structure and catalytic performance of SnO2-doped TiO_2 photocatalysts, Ceram. Int. (2014); 40 13305–13312. DOI: https://doi.org/10.1016/j.ceramint.2014.05.042.

20) Yang, C.; Huang, A.; Tang, A.; Zhang, X.; Yang, W. Microwave-assisted synthesis of ceria nanoparticles. Materials Research Bulletin, (2005);40 1690–1695. https://doi.org/10.1016/j.materresbull.2005.04.008

21) Yu, K. L.; Ruan, G. L.; Ben, Y. H.; Zou, J. J. Convenient synthesis of CeO_2 nanotubes. Materials Science and Engineering B, (2007); 139 197–200. https://doi.org/10.1016/j.mseb.2007.02.01.

22) Sharma, S., Graham, C., & Nino, J. C. Size-dependent structural and optical properties of CeO_2 nanocrystals. Journal of Applied Physics, (2010); 107(10), 103503. https://doi.org/10.1063/1.3359717

23) Bai, S., Li, D., Kong, R., Long, R., Wang, C., & Zeng, J. Monoclinic WO_3 nanostructures: Controlled synthesis, crystal structure, and photocatalytic performance.Materials Chemistry and Physics, (2019); 225, 112–119. https://doi.org/10.1016/j.matchemphys.2018.12.070

24) Huang, H., Xiao, Z., et al."CdS-TiO_2 Composites: Synthesis and Applications in Photocatalytic Degradation." Catalysis Today, (2021); 356, 398–409. DOI: https://doi.org/10.1016/j.cattod.2019.04.020.
25) D. Helm, H. Labischinski, G. Schallehn, et al., Classication and identication of bacteria by Fourier-transform infrared spectroscopy, J. Gen. Microbiol., (1991); 137, 69–79. DOI: https://doi.org/10.1099/00221287-137-1-69.
26) Martínez-de la Cruz, A., Sánchez-Martínez, D., & Cuéllar, E. L. Synthesis and characterization of WO_3 nanoparticles prepared by the precipitation method: Evaluation of photocatalytic activity under vis-irradiation. Solid State Sciences,(2010); 12(1) 88–94. https://doi.org/10.1016/j.solidstatesciences.2009.10.010.
27) Sanchez-Martinez, A., Koop-Santa, C., Ceballos-Sanchez, O., López-Mena, E. R., González, M. A., Rangel-Cobián, V., Orozco-Guareño, E., & García-Guaderrama, M. Study of the preparation of TiO_2 powder by different synthesis methods. Materials Research Express, (2019); 6(8) . https://doi.org/10.1088/2053-1591/ab21e8.
28) Fauzia, Khan, M. A., Chaman, M., & Azam, A. Antibacterial and sunlight-driven photocatalytic activity of graphene oxide conjugated CeO_2 nanoparticles. Scientific Reports, (2024);14(1), 6606. https://doi.org/10.1038/s41598-024-54905-0
29) Alterary, S. S., & El-Tohamy, M. F. Advanced Functionalized CeO_2/Al_2O_3 Nanocomposite Sensor for Determination of Opioid Medication Tramadol Hydrochloride in Pharmaceutical Formulations. Nanomaterials,(2022); 12(8), 1373.
30) Kumar, E., Selvarajan, P., & Balasubramanian, K. Preparation and Studies of Cerium Dioxide (CeO_2) Nanoparticles by Microwave-Assisted Solution Method. Recent Research in Science and Technology, (2010); 2(4), 420–425.
31) Govender, M. Structural and Optical Properties of WO_3 and its Gas Sensing Application (PhD thesis). University of Pretoria. Available at: (2014); http://hdl.handle.net/2263/46048.
32) Boga, B., Székely, I., Pap, Z., Baia, L., & Baia, M. Detailed spectroscopic and structural analysis of TiO_2/WO_3 composite semiconductors. Journal of Spectroscopy, 2018; Article ID 6260458. https://doi.org/10.1155/2018/6260458.
33) Pundir, S., Priya, R., Singh, K., Kaur, H., & Choudhary, P. A systematic study on synthesis of CeO_2 nanoparticles by various routes. IOP Conference Series: Earth and Environmental Science, (2023);1110(1), 012030. https://doi.org/10.1088/1755-1315/1110/1/012030
34) Raul, P. K., Senapati, S., Sahoo, A. K., Umlong, I. M., Devi, R. R., Thakur, A. J., & Veer, V. . CuO nanorods: A potential and efficient adsorbent in water purification. RSC Advances, (2014); 4(76), 40580–40587. https://doi.org/10.1039/c4ra04619f
35) M. Farahmandjou∗, M. Z. and T. P. F. of C. O. (CeO_2) nanoparticles using simple C. method. Synthesis of Cerium Oxide (CeO_2) nanoparticles using simple CO-precipitation method. Physical Chemistry Research, (2016); 496–499. DOI: 10.22036/pcr.2018.132220.1486
36) I. Ahmad, M. Usman, T.-K. Zhao, S. Qayum, I. Mahmood, A. Mahmood, A. Diallo, C. Obayi, F. I. Ezema, and M. Maaza Bandgap engineering of TiO2 nanoparticles through MeV Cu ions irradiation. Arab. J. Chem.(2020);13, 3344.
37) Raghupathi, K. R., Koodali, R. T., & Manna, A. C. Size-dependent bacterial growth inhibition and mechanism of antibacterial activity of zinc oxide

nanoparticles. Langmuir, (2011); 27, 4020–4028.

38) Dizaj, S. M., Lotfipour, F., Barzegar-Jalali, M., Zarrintan, M. H., & Adibkia, K. Antimicrobial activity of the metals and metal oxide nanoparticles. Materials Science and Engineering C, (2014); 44, 278–284.

39) Rai, M., Deshmukh, S. D., Ingle, A. P., & Gade, A. K. Silver nanoparticles: the powerful nanoweapon against multidrug-resistant bacteria and fungi. Journal of Applied Microbiology, (2012);112, 841–852.

40) Sirelkhatim, A., Mahmud, S., Seeni, A., et al. Review on zinc oxide nanoparticles: antibacterial activity and toxicity mechanism. Nano-Micro Letters,(2015); 7, 219–242.

41) Hoseinzadeh, E., Makhdoumi, P., Taha, P., et al. A review on nano-antimicrobials: metal nanoparticles, polymeric nanoparticles, carbon nanostructures and their mechanisms of action. Journal of Industrial and Engineering Chemistry, (2017); 44, 1–17.

42) Ghotekar, S., Pansambal, S., Oza, R., et al. Bio-green synthesis of TiO_2 nanoparticles and their antifungal activity. Materials Today: Proceedings, (2020); 23, 63–68.

43) Suresh, D., Nethravathi, P. C., Rajanaika, H., et al. Green synthesis of multifunctional zinc oxide nanoparticles using Cassia fistula flower extract and their antimicrobial activity. Spectrochimica Acta Part A, (2015); 141, 128–134.